

# Measurement of variability dynamics in cortical spike trains

Martin P. Nawrot<sup>a,b,1</sup>, Clemens Boucsein<sup>a,b</sup>, Victor Rodriguez Molina<sup>b,2</sup>,  
Alexa Riehle<sup>c</sup>, Ad Aertsen<sup>a,b</sup>, Stefan Rotter<sup>a,d,\*</sup>

<sup>a</sup> Bernstein Center for Computational Neuroscience Freiburg, Germany

<sup>b</sup> Neurobiology & Biophysics, Faculty of Biology, University of Freiburg, Germany

<sup>c</sup> Institut de Neurosciences Cognitives de la Méditerranée – CNRS & Université Aix-Marseille 2, Marseille, France

<sup>d</sup> Theory & Data Analysis, Institute for Frontier Areas of Psychology and Mental Health, Freiburg, Germany

Received 7 May 2007; received in revised form 5 October 2007; accepted 13 October 2007

## Abstract

We propose a method for the time-resolved joint analysis of two related aspects of single neuron variability, the spiking irregularity measured by the squared coefficient of variation ( $CV^2$ ) of the ISIs and the trial-by-trial variability of the spike count measured by the Fano factor (FF). We provide a calibration of both estimators using the theory of renewal processes, and verify it for spike trains recorded *in vitro*. Both estimators exhibit a considerable bias for short observations that count less than about 5–10 spikes on average. The practical difficulty of measuring the  $CV^2$  in rate modulated data can be overcome by a simple procedure of spike train demodulation which was tested in numerical simulations and in real spike trains. We propose to test neuronal spike trains for deviations from the null-hypothesis  $FF = CV^2$ . We show that cortical pyramidal neurons, recorded under controlled stationary input conditions *in vitro*, comply with this assumption. Performing a time-resolved joint analysis of  $CV^2$  and FF of a single unit recording from the motor cortex of a behaving monkey we demonstrate how the dynamic change of their quantitative relation can be interpreted with respect to neuron intrinsic and extrinsic factors that influence cortical variability *in vivo*. Finally, we discuss the effect of several additional factors such as serial interval correlation and refractory period on the empiric relation of FF and  $CV^2$ .

© 2007 Elsevier B.V. All rights reserved.

**Keywords:** Coefficient of variation; Cortical variability; Gamma process; Fano factor; Monkey motor cortex; Noise current injection; Renewal process, Spiking irregularity

## 1. Introduction

Variability of neural activity is apparent throughout the central nervous system, in all types of electrophysiological signals. In the mammalian brain, the degree of variability at the single-neuron level increases with the stages of sensory processing, being lowest in the periphery and highest in cortical structures (Kara et al., 2000). Likewise, variability is also lower in the motor periphery than in the cortex (Prut and Perlmutter, 2003). Understanding the nature and the origin of

the observed high variability in the neocortex is essential for our understanding of the neural code used for representation and processing of information in cortical networks (Stein et al., 2005).

Two types of single neuron variability are usually distinguished, reflecting variability on different time scales. Spike train irregularity (Holt et al., 1996; Softky and Koch, 1993; Teich et al., 1997) refers to the random appearance of the sequence of action potentials which is statistically expressed in the variance and the coefficient of variation (CV) of inter-spike intervals (ISI). It signifies *intra-trial variability* on a relatively short time scale, determined by the typical ISI, i.e. in the range of tens to hundreds of milliseconds. By contrast, the *trial-by-trial variability* is measured by the variance and the Fano factor (FF) of the spike count across repeated observations that may be separated by long time intervals (Shadlen and Newsome, 1998; Teich et al., 1997).

Here, we propose an approach to the investigation of single neuron spike train variability that can help to distinguish

\* Corresponding author at: Institute for Frontier Areas of Psychology and Mental Health, Wilhelmstraße 3a, D-79098 Freiburg, Germany.  
Tel.: +49 761 207 2121; fax: +49 761 207 2191.

E-mail address: stefan.rotter@biologie.uni-freiburg.de (S. Rotter).

<sup>1</sup> Current address: Neuroinformatics and Theoretical Neuroscience, Institute of Biology-Neurobiology, Free University Berlin, Germany.

<sup>2</sup> Current address: Facultad de Medicina, Fisiología, Universidad Autónoma del Estado de Morelos, Cuernavaca, Mexico.

different contributing factors to the observed single neuron variability *in vivo*. Central to our approach is the null-hypothesis  $FF = CV^2$ , a theoretic result for renewal models which are briefly reviewed in the method section. We confirmed this prediction for cortical pyramidal neurons *in vitro* in a series of current injection experiments where we mimicked stochastic inputs assuming stationary network conditions. For variability studies *in vivo* we suggest to jointly analyse both aspects of variability in a time-resolved manner to uncover task-related modulations and to detect periods of significant deviation from the equality of FF and  $CV^2$ . This is shown for an example of single-unit recordings from motor-cortical neurons in a behaving monkey. In the discussion we resume potential interpretation for such deviation and discuss sources for the observed high variability of cortical activity *in vivo*. Preliminary results of this study were presented in abstract form (Nawrot et al., 2001; Rotter et al., 2005).

## 2. Methods

### 2.1. Point process theory

We briefly review several aspects of point process theory that are relevant for the methods and introduce the concept of operational time that provides the means for the analysis of spike train irregularity in rate-modulated processes.

#### 2.1.1. Renewal point processes

Stochastic point processes are frequently employed as mathematical models for neuronal spiking (e.g. Johnson, 1996; Perkel et al., 1967a, b; Tuckwell, 1988). Of particular interest is the class of renewal processes (Cox, 1962). Here, the intervals  $X_i$  between successive points (i.e. spikes) are independent and identically distributed (i.i.d.) with a fixed interval distribution  $f(x)$ , implying a constant point process intensity, or spike rate. Renewal models of spiking can be defined by specifying an arbitrary interval distribution. One prominent example is the Poisson process. Its points occur at constant rate in a completely random fashion and independent of each other. It exhibits an exponential interval distribution, while the number of points encountered during a finite observation interval is Poisson distributed. Another prominent example for a renewal process is the spiking of an integrate-and-fire model neuron with stationary Poissonian inputs where the inter-spike interval distribution depends both on the detailed biophysical properties of the model and on the synaptic input it receives (Burkitt, 2006; Lindner, 2004; Tuckwell, 1988).

The experimental setting in which neuronal activity is recorded in behaving animals typically involves repeated trials. The respective observation period is usually aligned to a temporal marker, e.g. the presentation of a stimulus or the occurrence of a behavioral event. Thus, the start of the observation interval generally represents a ‘random point’ with respect to neuronal spiking, and generally does not coincide with a spike event. For a renewal process, this implies that the time  $X_0$  up to the first observed event has a probability density function (p.d.f.)

$\mathcal{F}(x)/\mu$ , where

$$\mathcal{F}(x) = Pr(X > x) = \int_x^\infty f(u) du$$

is the survivor function, and  $\mu$  is the mean interval given by first moment of  $f(x)$ . All other intervals  $X_1, X_2, \dots$  have p.d.f.  $f(x)$ . If these criteria are met we speak of an *equilibrium* renewal process.

In special cases, however, the start of observation in each trial might coincide with a spike event at time  $t = 0$  (see Section 4). Then one speaks of an *ordinary* renewal process (Cox, 1962; Cox and Isham, 1980; Tuckwell, 1988). Throughout this manuscript we refer to the equilibrium situation when using the term ‘renewal process’ without further specification.

#### 2.1.2. Gamma processes

Gamma processes are closely related to the Poisson process, with an extra parameter that allows for the adjustment of regularity of its pulse trains. For this reason, they have frequently been used as a model for neuronal spiking (Baker and Gerstein, 2001; Nawrot et al., 2003a; Pauluis and Baker, 2000; Reich et al., 1998; Stein, 1965; Tuckwell, 1988). In a number of studies, the gamma process was fitted to experimental data and compared to other models (Baker and Lemon, 2000; Brown et al., 2001; Nawrot, 2003; Teich et al., 1997). They typically feature a relative refractory period of low spike probability following each event (cf. Fig. 3). However, since the p.d.f. of a gamma distribution is strictly positive for all  $x > 0$ , it does not incorporate an absolute refractory period during which the spike probability is zero.

The gamma process has the interval density

$$f_{\alpha,\rho}(x) = \begin{cases} \frac{1}{\Gamma(\alpha)} \rho(\rho x)^{\alpha-1} e^{-\rho x}, & x \geq 0, \\ 0, & x < 0, \end{cases}$$

where  $\Gamma$  denotes the gamma function, and  $\alpha > 0$  and  $\rho > 0$  are its two parameters. The mean interval  $\mu$  and associated rate  $\lambda$  of the process are given by

$$\mu = E[X] = \frac{\alpha}{\rho} \quad \text{and} \quad \lambda = \frac{1}{\mu} = \frac{\rho}{\alpha}.$$

The variance of the interval distribution is given by

$$\text{Var}[X] = \frac{\alpha}{\rho^2}.$$

The squared coefficient of variation of the inter-spike interval distribution

$$CV^2[X] = \frac{\text{Var}[X]}{E[X]^2} = \frac{1}{\alpha}$$

specifies the relative width of the p.d.f. and, therefore, was used to parameterize the irregularity of the process. The Poisson process represents the special case  $\alpha = 1$ , for which the p.d.f. is the exponential distribution. For  $\alpha > 1$ , the process is more regular, while for  $0 < \alpha < 1$  the process is more irregular than the Poisson process, and events appear clustered in time.

In this manuscript we employed equilibrium gamma processes to investigate and calibrate statistical measures of interval and counting statistics both by means of analytical treatment and numerical simulations. To ensure equilibrium conditions in numerical simulations of gamma processes we allowed for an appropriate warm-up by starting the simulation some time before the actual measurement began. Alternatively, we started our simulation by drawing the first interval  $X_0$  from the appropriate length biased distribution  $\mathcal{F}_{\alpha,\rho}(x)/\mu$ . This was conveniently achieved by a product  $UY$  of two independent random numbers, where  $Y$  had p.d.f.  $f_{\alpha+1,\rho}(y)$ , and  $U$  was uniformly distributed on  $[0, 1]$ . All numerical simulations were performed with *Matlab* (The MathWorks, Inc.). Parts of the analytical calculations were performed with the help of *Mathematica* (Wolfram Research, Inc.). We provide documented Matlab code for some of the methods described below within the framework of the FIND toolbox (Meier et al., 2007; <http://find.bccn.uni-freiburg.de>).

### 2.1.3. Operational time and rate modulation

Neurons observed in a living organism typically exhibit temporal changes of their firing rates in response to sensory input, or in relation to behavior. This important feature of neuronal processing can be captured by rate modulated renewal processes, where the process intensity is no longer constant but defined through a (deterministic) function of time. We start with the well-known concept of a non-homogenous Poisson process (Cox and Isham, 1980; Kass and Ventura, 2001; Tuckwell, 1988) for which the intensity is no longer constant in time, but has a time course  $\lambda(t) \geq 0$ . The number  $N$  of events in repeated observations during a given interval  $(a, b)$  is Poisson distributed

$$Pr(N = k) = \frac{1}{k!} \left[ \int_a^b \lambda(s) ds \right]^k e^{-\int_a^b \lambda(s) ds} \quad (k = 0, 1, 2, \dots) \quad (1)$$

Operational time  $t'$  is defined by the non-linear transformation of real time  $t$  as

$$t' = \Lambda(t) = \int_0^t \lambda(s) ds, \quad (2)$$

which is one-to-one if  $\lambda(t)$  is strictly positive (Gestri and Petracchi, 1970). In case of a constant intensity this simplifies to a multiplication of the event times with the intensity. Evidently, in operational time, which is dimensionless, the process is stationary with unit rate and has a mean interval  $\mu' = 1$ . The expected number of events in  $(a, b)$  then amounts to

$$E[N] = b' - a' = \int_a^b \lambda(s) ds. \quad (3)$$

The concept of operational time is also of practical use in simulating a non-homogenous Poisson process. First, a stationary realization  $t'_1 < t'_2 \dots < t'_N$  is produced in operational time with intervals  $X'_i = t'_{i+1} - t'_i$  drawn from the exponential distribution with unit mean. In a second step, the inverse transformation is applied to each single event of the realization:

$$\Lambda^{-1}(t') = \min\{t | \Lambda(t) \geq t'\}. \quad (4)$$

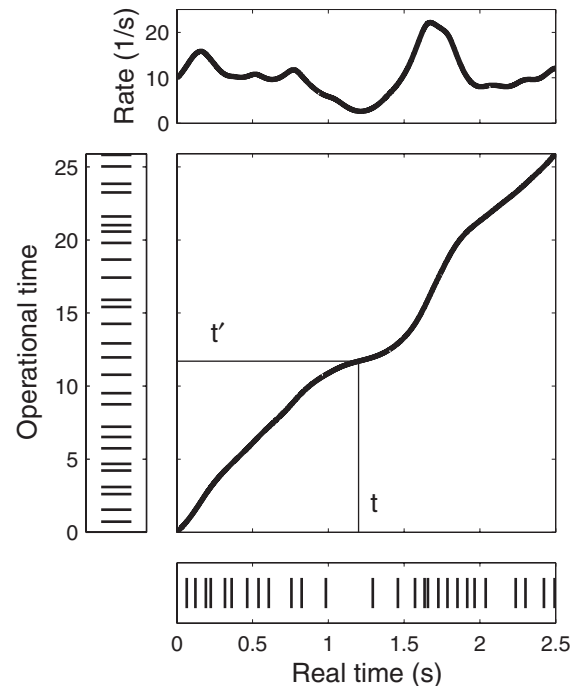


Fig. 1. Transformation of time. A renewal process of unit rate is simulated in operational time (vertical panel). A spike event at time  $t'$  is translated into a spike event in real time  $t$  by the time transformation (center panel, Eq. (2)) given by the integral of the rate function (top panel). Conversely, a rate modulated realization of a point process may be demodulated by mapping an event in real time  $t$  onto the corresponding event in operational time  $t'$ .

A similar procedure is applied to transform uniform random variables to variables with arbitrary distributions (see Ripley, 1987). The rate modulated, or non-homogenous renewal process generalizes this concept (Baker and Lemon, 2000; Barbieri et al., 2001; Berry and Meister, 1998; Brown et al., 2001; Oata, 1988; Oram et al., 1999; Reich et al., 1998; Truccolo et al., 2005). Let  $f(x')$  denote the p.d.f. for an arbitrary interval distribution in operational time  $t'$ , and let  $\lambda(t)$  be the rate profile of the process in real time. Again we first generate a realization in operational time on the basis of  $f(x')$  and then ‘warp’ the time axis according to the inverse transformation given by Eq. (4) (Fig. 1). Generally, such transformation of independent stochastic variables results again in an independent set of variables. By construction, intervals are still mutually independent but no longer identically distributed. In fact, the waiting time distribution of the next upcoming event depends on the time course of the rate function since the most recent event. Note that falsely assuming identically distributed intervals (i.e. constant rate) when analyzing the resulting sequence of intervals would result in serial correlations among intervals which are, in fact, a reflection of the time-varying rate function.

Conversely, given such rate-modulated renewal process with a time-varying rate function  $\lambda(t)$  (e.g. estimated by a peri-stimulus time histogram) we can ‘un-warp’ real time to operational time by applying the transformation given by Eq. (2). As we will show, this latter procedure can be successfully employed to obtain estimates of interval statistics from neuronal responses with non-stationary firing rates.

Note that our approach is to estimate the trial-averaged so-called *unconditional* rate function from repeated trials without making any assumptions about the spiking model before we rescale the time axis. In a second step we then estimate statistical parameters from the transformed spike trains. A somewhat different approach has been suggested by Barbieri et al. (2001) and Brown et al. (2001) where the *conditional* intensity function is estimated directly from single trial spike data. If this model is accurate, the respective transformation of the individual spike train will result in a homogenous Poisson process. Spike train variability may then be computed for the estimated model (Barbieri et al., 2001; Brown et al., 2001; Wiener, 2003).

#### 2.1.4. Empirical measures of irregularity and variability

Consider an observation interval  $(a, b]$  with  $a < b$  and duration  $T = b - a$ . Let  $a < t_1 < t_2 < \dots < t_N \leq b$  denote a train of  $N$  spikes that occurred during one particular observation. Then,  $X_1, X_2, \dots, X_{N-1}$  is the sequence of the  $N - 1$  observed inter-spike intervals  $X_i = t_{i+1} - t_i$ . Multiple independent repetitions of the same experiment result in an ensemble of spike trains, each with its count of spikes  $N_j$ . Irregular spiking is expressed by a variable length of the inter-spike interval  $X$ . As a quantitative measure of this irregularity we employ the squared coefficient of variation of the ISIs gathered during observations of length  $T$

$$CV^2 = \frac{\text{Var}[X]}{E[X]^2}.$$

Variability of activity across multiple observations or repeated trials expresses itself by a variable spike count  $N$ . We use the Fano factor (Fano, 1947):

$$FF = \frac{\text{Var}[N]}{E[N]}$$

to quantify the normalized count variance across repeated observations of length  $T$ . The  $CV^2$  measures neuronal variability of intervals collected within observation on a relatively short time scale which is comparable to the length of the typical ISI. The Fano factor captures variability on a considerably longer time scale. It refers to spike count observations of length  $T$  and measures the spread of this number across repeated observation trials, which may be separated by pauses that are large compared to  $T$ . The quantities  $CV^2$  and FF, however, are by no means independent variables. Under stationary conditions, a given degree of spike timing irregularity (short-term) implies a certain amount of spike count variability (long-term), and *vice versa*. In particular, for a stationary renewal process in equilibrium it holds that

$$FF = CV^2 \quad (5)$$

for the limit of long observations (Cox, 1962; Cox and Lewis, 1966; Ratnam and Nelson, 2000; Tuckwell, 1988). A deviation from this equality indicates a deviation from the stationary renewal model which cannot be easily detected if only one aspect of variability is analyzed alone. We will show that in experimental spike trains it can thus be very useful to compare interval and count variability as estimated in the same observation window.

The theoretical relation of interval and count variability in point process theory marks the major advantage of the  $CV^2$  over other measures of irregularity.

#### 2.2. In vitro current injection experiments

We performed a series of *in vitro* experiments where we stimulated regular spiking layer 5 pyramidal neurons of neocortex by means of somatic injection of fluctuating currents that mimicked synaptic input from a large number of presynaptic neurons.

Acute slices of 400  $\mu\text{m}$  thickness were prepared from sensorimotor cortex of rats (Long-Evans, P15–P28) as described previously (Boucsein et al., 2005). Whole cell patch recordings (pipette resistance 2–6  $\text{M}\Omega$ ) were made from layer 5 pyramidal neurons which were identified visually using infrared video microscopy (Dodt and Zieglgänsberger, 1990). Current control signals were sampled at 20 kHz and low-pass filtered at 3–10 kHz before application. Voltage recordings were low-pass filtered at 3–5 kHz using an Axoclamp 2B amplifier (Axon Instruments, Foster City, CA), and sampled at 10–20 kHz using a CED-1401 Plus device (Cambridge Electronic Design, Cambridge, UK). Only regular spiking neurons ( $n = 17$ ) were considered for analysis.

Synaptic input currents were synthesized as a superposition of excitatory and inhibitory postsynaptic currents (EPSCs and IPSCs). Single PSCs were modeled as decaying exponentials with amplitudes of  $\pm 30$  pA and decay time constants of 3 ms or 6 ms for EPSCs and IPSCs. The total charge carried by a single PSC thus amounted to 0.09 and  $-0.18$  pC, respectively. In a first set of experiments we injected traces of fluctuating input current with a total duration of either 300 s or 1200 s. We assumed independent pools of excitatory and inhibitory presynaptic neurons, each firing with a stationary rate and obeying Poissonian statistics. After convolution with the EPSC and IPSC waveform, respectively, the resulting excitatory and inhibitory shotnoise currents were added, yielding a single current trace (Fig. 2a). In the standard protocol, excitation was counterbalanced by 50% inhibition, leading to a ratio of mean total inhibition to mean total excitation of  $r_i = 0.5$  (Stevens and Zador, 1998). In an alternative protocol we assumed purely excitatory input ( $r_i = 0$ ). The net depolarizing input current was calibrated such that  $I_{\text{net}} = I_{\text{exc}} + I_{\text{inh}} = 100$  pA. Thus, for  $r_i = 0.5$  input rates amounted to about 2000 excitatory and 500 inhibitory spikes per second. At the beginning of each recording we adjusted the effective current amplitude for each individual neuron to yield comparable sustained response spike rates in the range of 4–14 spikes/s (cf. Fig. 2b). Before current injection the neurons did not show spontaneous spiking due to the limited spontaneous network input in the slice preparation. Therefore, the first 50 s of spiking activity following the onset of current injection were discarded from analysis, allowing for a ‘warm-up’ time that should allow the neuron to adapt to the increased input and to settle in a renewed state of equilibrium.

In a second set of experiments, the injected synthetic currents reflected a defined temporal modulation of the synaptic input. We constructed 20 trials of 5 s length each. Background input

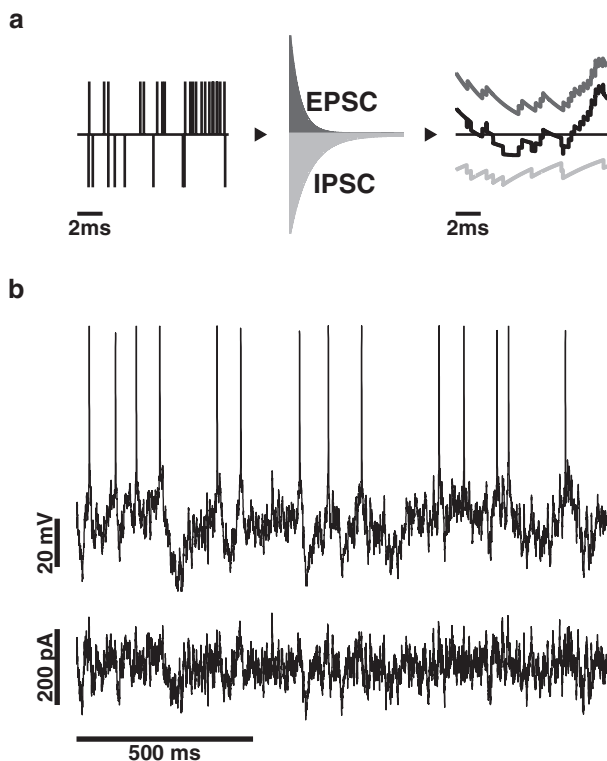


Fig. 2. Noise current injection. (a) Excitatory (top) and inhibitory (bottom) presynaptic events were generated as independent Poisson processes. Each event contributed a single EPSC or IPSC to the total current (black curve), carrying a net charge of 0.09 and  $-0.18$  pQ, respectively. (b) Membrane potential of a layer 5 pyramidal cell (top) measured during the injection of a fluctuating current (bottom) that replaced excitatory and inhibitory synaptic input.

was modeled as stationary excitatory and inhibitory Poisson processes with inhibition ratio of  $r_i = 0.5$  and net background current of  $I_{\text{net}} = 200$  pA, equivalent to excitatory and inhibitory rates of about 4000 and 1000 spikes/s, respectively. In each trial we added to this a bell-shaped temporal modulation of the excitatory input rate before realizing and convolving the spike trains with the EPSC kernel. We chose a Gaussian profile with a latency of 2.5 s, amplitude 200 pA and standard width of either 200 or 300 ms. These trials were interlaced with 20 control trials of identical length that did not exhibit any temporal modulation of the input. All trials were then concatenated, yielding a single long current trace of 200 s duration. Again, this was prepended by a warm-up period (100 s).

### 2.3. Monkey experiment

After the monkey had successfully learned the task ( $> 85\%$  correct performance; see Grammont and Riehle, 2003), a cylindrical stainless steel recording chamber (inner diameter: 15 mm) was implanted above the primary motor cortex under aseptic conditions and general halothane anesthesia ( $< 2.5\%$  in air). A stainless steel T-bar was cemented to the skull to fixate the animal's head during recording sessions. A multi-electrode microdrive (Reitböck system, Thomas Recording, Germany) was used to transdurally insert seven quartz-glass

insulated platinum–tungsten electrodes (outer diameter:  $80\mu\text{m}$ , impedance:  $2\text{--}5$  M $\Omega$  at 1 kHz). The electrodes were arranged in a circle, one in the middle and 6 around it (equally spaced at  $330\mu\text{m}$ ). From each electrode, electrical signals were amplified and band-pass filtered (0.3–10 kHz). Action potentials of one single neuron per electrode were then isolated by using a window discriminator. Neuronal signals along with behavioral events (trial start and end, target information, reaction and movement times, reward, errors) were stored for off-line analysis with a time resolution of 1 kHz.

## 3. Results

### 3.1. Bias and variance of estimation

#### 3.1.1. Spike train irregularity

Empirical estimates of inter-spike interval statistics depend on the length of the observation. Suppose an equilibrium renewal process with interval density  $f(x)$  is observed over a finite time interval  $(a, b]$  of duration  $T = b - a$ . Evidently, we can only observe intervals  $X$  that are shorter than the observation interval  $T$ , i.e.  $\hat{f}(x) = 0$  for  $x > T$ . On the other hand, the encounter of very short intervals  $x \ll T$  is essentially unaffected by the finite-length observation window. This effect is commonly known as right-censoring (e.g. Wiener, 2003). We give here an approximate expression for the interval distribution  $\hat{f}(x)$  corresponding to this experiment. For all intervals  $x \in (0, T)$ , the likelihood of their observation is proportional to  $T - x$ , the ‘free space’ left in the observation window. This leads to the expression:

$$\hat{f}(x) = \begin{cases} \eta^{-1} (T - x) f(x), & \text{for } x \in [0, T], \\ 0, & \text{otherwise,} \end{cases} \quad (6)$$

where

$$\eta = \int_0^T (T - s) f(s) ds$$

is a normalization constant. If  $\mu$  is the mean interval,  $\eta$  approaches  $T - \mu$  for large observation windows  $T \gg \mu$ .

In Fig. 3a we compared the full analytic gamma distribution  $f(x)$  of order  $\alpha = 2.8$  (light gray) with the analytically derived distribution  $\hat{f}(x)$  based on observations within an interval of length  $T = 1.5$  (dark gray). Fig. 3b shows an ISI histogram extracted from neuronal spike trains measured *in vitro*. The full distribution (light gray) was sampled from a very long record comprising 4181 intervals in total. Sampling the same spike train by using short observation intervals of length  $T' = 1.5$  in operational time shows the same effect as for the gamma model: The resulting interval distribution is squeezed, and both its mean and its variance are reduced.

The distortion of the ISI distribution is more pronounced for shorter observations. Conversely, for a fixed observation length  $T$ , the effect becomes stronger for a larger mean interval  $\mu$  or, equivalently, for a lower spike rate. According to Eq. (6), we can partially correct for the introduced distortion by multiplying  $\hat{f}(x)$  with  $1/(T - x)$  on the interval  $[0, T)$  (red curves in Fig. 3). This correction allows us to fit empirical data to a model

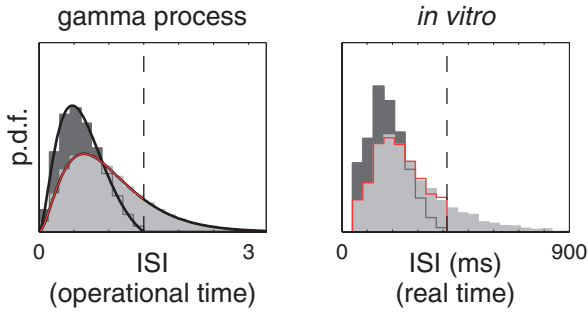


Fig. 3. Inter-spike interval distribution for finite observation time. Analytical and simulated distributions for a gamma-process (left) and empirical distributions from a layer 5 pyramidal neuron recorded *in vitro* (right). The light gray histogram in the left panel displays the probability density  $f(x)$  constructed from  $10^5$  intervals randomly drawn from a gamma distribution ( $\alpha = 2.8$ ). The dark gray histogram shows the modified distribution  $\hat{f}(x)$  for a finite observation interval of length 1.5 in operational time. Solid lines show the corresponding analytical results (Eqs. (3) and (6)). The gamma order of 2.8 was estimated as  $\alpha = 1/\text{CV}^2$  from the full distribution *in vitro* (light gray histogram, right), constructed from 4181 intervals recorded during 1150 s. Short observations of length 415 ms (1.5 times the mean interval length) yielded the dark gray *in vitro* histogram.

distribution on the restricted interval  $[0, T)$  and, for instance, to extract the order of a gamma model. It does not, however, allow for an unbiased ‘model-free’ estimation of mean, variance and squared coefficient of variation.

We calibrated the influence of the observation length  $T$  on the estimated values of mean interval, variance and  $\text{CV}^2$  for gamma processes of various orders. Fig. 4, left panels, shows the analytic results (gray lines) which were confirmed by numeric simulations (dotted lines). For increasing width of the analysis window, the  $\text{CV}^2$  approaches the asymptotic value (Cox, 1962; Cox and Lewis, 1966):

$$\text{CV}_{\infty}^2 = \frac{1}{\alpha}. \quad (7)$$

In the case of a Poisson process (dashed gray line) the curve saturates beyond  $T' = 10$ , i.e. for an expected spike count of about 10 within the analysis window (Eq. (3)). The more regular processes ( $\alpha > 1$ ) reach the asymptotic level faster, while the more irregular processes ( $\alpha < 1$ ) approach it more slowly.

For experimental spike trains recorded under stationary input conditions (see Section 2) we observed the same general bias with respect to the length of the observation interval. Fig. 4, right panels, shows the data from five neurons. All neurons exhibited spiking which was more regular than Poisson, comparable to a gamma process of order 2–4.

Estimates of spike train irregularity from finite length experimental observations (squared coefficient of variation of the ISIs) suffer from a general tendency to under-estimate its value. One should use ‘long enough’ observation windows  $T \gg \mu$  to avoid a considerable bias. Our results suggest to use windows that comprise at least 5–10 spikes. For any specific set of experimental data, information can be gained from calibration curves as shown in Fig. 4, which depict the dependence of the bias on observation time.

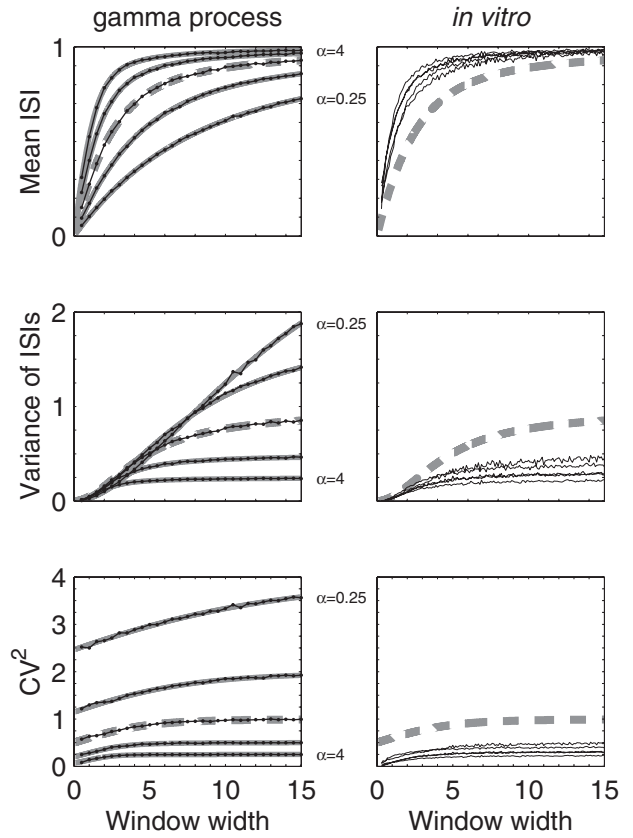


Fig. 4. Dependence of interval statistics on observation length. All times are specified in operational time. For gamma processes (left), all three statistical measures of mean interval  $\mu$  (top), variance of intervals  $\sigma^2$  (middle), and squared coefficient of variation  $\text{CV}^2$  (bottom) show a monotonic dependence on the width  $T'$  of the analysis window. Shown are the analytic (gray lines) and simulation (thin black lines) results for gamma processes of order  $\alpha = 0.25, 0.5, 1, 2, 4$ . In the right panels we show the empiric results from five pyramidal neurons that were stimulated with mixed excitatory/inhibitory shotnoise currents. The more irregular the process is, the more slowly the  $\text{CV}^2$  approaches the asymptotic limit of  $1/\alpha$  for  $T' \rightarrow \infty$ . The Poisson process (dashed gray line) saturates at about  $T' = 10$ . For stationary input the cortical neurons *in vitro* typically exhibited a more regular spiking than a Poisson process. The curves saturate for about 5–7 units of operational time.

### 3.1.2. Spike count variability

Count variance and the Fano factor are also subject to an estimation bias which depends on the length  $T$  of the observation interval. We give here an analytic expression for this dependency. Let

$$x(t) = \sum_i \delta(t - t_i)$$

denote a (random) spike train with spikes at times  $t_i$ . We assume that the generating process is stationary and has a finite rate

$$E[x(t)] = \lambda = \frac{1}{\mu} < \infty.$$

Let

$$N_T = \int_0^T x(t) dt$$

denote the number of events in  $(0, T]$ . We then have, by linearity of the expectation:

$$E[N_T] = \int_0^T E[x(t)] dt = \lambda T. \quad (8)$$

Similarly, writing  $\tilde{x}(t) = x(t) - \lambda$ , we obtain

$$\begin{aligned} \text{Var}[N_T] &= E[(N_T - \lambda T)^2] \\ &= E \left[ \left( \int_0^T \tilde{x}(t) dt \right)^2 \right] \\ &= E \left[ \left( \int_0^T \tilde{x}(t) dt \right) \left( \int_0^T \tilde{x}(u) du \right) \right] \\ &= E \left[ \left( \int_0^T \int_0^T \tilde{x}(t) \tilde{x}(u) dt du \right) \right] \\ &= \int_0^T \int_0^T E[\tilde{x}(t) \tilde{x}(u)] dt du \\ &= \int_0^T \int_0^T \text{Cov}[x(t), x(u)] dt du. \end{aligned}$$

Since the process is stationary, its auto-covariance will depend only on the time lag, and not on the time of its evaluation:

$$\text{Cov}[x(t + \Delta), x(t)] = \gamma_{xx}(\Delta).$$

The above double integral can be simplified by the substitution  $\Delta = t - u$  and  $s = (t + u)/2$ , yielding

$$\begin{aligned} \text{Var}[N_T] &= \int_{-T}^T \int_{|\Delta|/2}^{T-|\Delta|/2} \gamma_{xx}(\Delta) ds d\Delta \\ &= \int_{-T}^T [T - |\Delta|] \gamma_{xx}(\Delta) d\Delta. \end{aligned} \quad (9)$$

Let  $f(t)$  be the p.d.f. of the ISIs, which in the case of a renewal process are independent and identically distributed. Let  $\mu$  and  $\sigma^2$  denote their mean and variance, respectively. Let further  $f_r(t)$  denote the p.d.f. of an  $r$ -fold sum of independent intervals, given by the convolution:

$$f_r(t) = \underbrace{(f * \dots * f)}_{r\text{-times}}(t).$$

We define  $f_0(t) = \delta(t)$ . The auto-covariance of the process is then given by

$$\gamma(\Delta) \equiv \text{Cov}[x(t + \Delta), x(t)] = \frac{1}{\mu} \sum_{r=0}^{\infty} f_r(|\Delta|) - \frac{1}{\mu^2}.$$

Thus, for any given renewal process specified by its ISI distribution, we are now in the position to (numerically) compute the explicit dependence of the count variance and, therefore, of the Fano factor on the observation length  $T$ .

In the special case of a Poisson process, the counts are Poisson distributed for all values of  $T$ . The count variance is then equal to the mean count, and thus the Poisson process has Fano factor

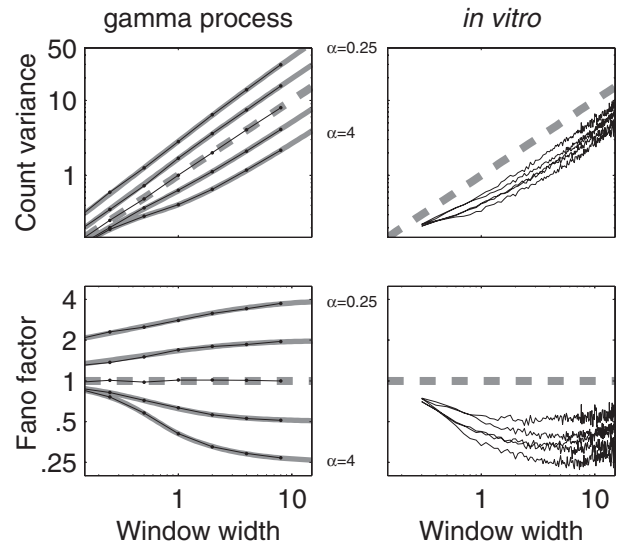


Fig. 5. Dependence of count statistics on observation length. (Left) The gray lines indicate the analytic solutions for the gamma process ( $\alpha = 0.25, 0.5, 1, 2, 4$ , top to bottom), the thin black lines show the corresponding simulation results. The variance of the Poisson process (gray dashed line) is equal to the expected mean count corresponding to the operational time on the abscissa Eq. (2). The Fano factor of the Poisson process is equal to 1, irrespective of the observation length  $T'$ . For short observation intervals ( $T' \rightarrow 0$ ), the estimation tends to unity, irrespective of  $\alpha$ . For large  $T'$ , the Fano factor monotonically approaches the asymptotic value of  $1/\alpha$ , saturating for all gamma orders at about  $T' = 10$ . (Right) Calibration for the same five recordings as presented in Fig. 4. The count variance of the neuronal process exhibits a behavior that is very similar to the more regular point processes with gamma orders  $\alpha \geq 2$ .

FF = 1, independently of the observation length. For general renewal processes, the situation is different. Only in the limit of long observations, one has (Cox, 1962)

$$\text{Var}[N_T] \sim \frac{\sigma^2}{\mu^3} T, \quad (10)$$

which, together with Eq. (8), leads to the equality in Eq. (5).

In Fig. 5, left panels, we show the estimation bias for the count variance and the Fano factor for gamma processes of various orders  $\alpha$ , as a function of observation length  $T'$  in operational time. In addition to the analytically obtained curves (gray lines; based on Eq. (9)) we performed numerical simulations (thin black lines), calculating the mean of  $10^4$  independent observations. For increasing window size  $T'$ , the function of count variance quickly approached the linear relation given by Eq. (10), resulting in straight lines with slope 1 on the double-logarithmic scale for both the analytical solution and numerical simulations. The Fano factor saturated at the asymptotic level of  $1/\alpha$  at  $T' \approx 10$ , independently of the gamma order. Note that for shorter intervals the Fano factor tends to unity, irrespective of the gamma order (Ratnam and Nelson, 2000). Thus, for processes more regular than the Poisson process ( $\alpha > 1$ ) there is a tendency to over-estimate the count variability, for processes less regular than the Poisson process ( $\alpha < 1$ ) the opposite is the case. By contrast, the bias in estimating the interval irregularity is always negative (Fig. 4).

In the right panels of Fig. 5 we investigated how the count variance and the Fano factor depend on observation time

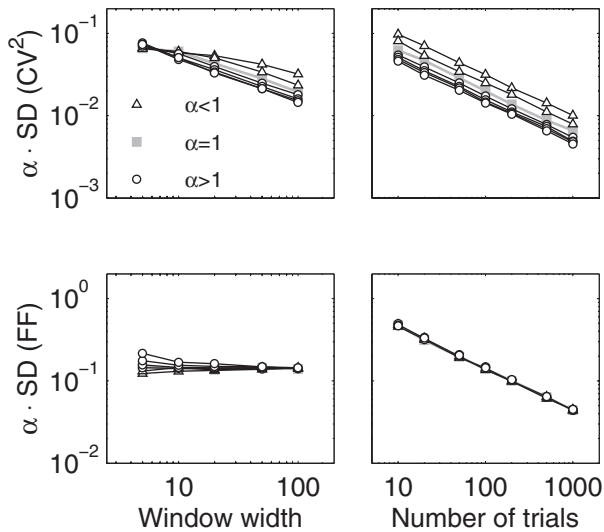


Fig. 6. Variance of estimation. The calibration is based on simulated ensembles of gamma processes. The standard deviation of estimating CV<sup>2</sup> (top) and FF (bottom) is approximately inversely proportional to the gamma order  $\alpha$ . Increasing the observation length  $T'$  increases the average number of ISIs and, therefore, decreases the standard deviation of the CV<sup>2</sup> estimator (top left), but does not influence the reliability of the FF estimator (bottom left). With an increasing number of trials  $N$  (right panels), the standard deviation decreases as  $1/\sqrt{N}$  for both estimators. The estimation error is generally smaller for the CV<sup>2</sup> (top) than for the FF (bottom). In the left panels we used a fixed  $N = 100$ , in the right panels we used a fixed window width  $T' = 100$ .

in cortical pyramidal neurons. As for the CV<sup>2</sup>, all neurons behaved similar to a gamma process of order 2–4 and we may again obtain a reasonable good estimate for observation intervals that show an average spike count on the order of 5–10 spikes.

For all stochastic point processes – except for the homogeneous Poisson process, but including the Poisson processes with a dead-time – the Fano factor exhibits a significant bias for short observations. Under mild regularity assumptions, a value of FF = 1 is approached for  $T' \rightarrow 0$ .

Note, that the dependence of FF on the observation length is not necessarily monotonic (e.g. for gamma processes of high order, data not shown). Several properties of mathematical or operationally defined point processes, including biophysically inspired neuron models, have a bearing on this dependence, for example the feature of an absolute refractory period (see Section 4).

### 3.1.3. Variance of the estimator

So far we calibrated the estimators for CV<sup>2</sup> and FF only with respect to their expectation value. We now focus on the variance of the estimator itself. In practical terms this is of interest because we want to have some idea about how reliable our estimates of interval or count variability can be. For this we repeatedly simulated spike train ensembles of a gamma process and estimated FF and CV<sup>2</sup>. In Fig. 6, the standard deviation of the estimates multiplied with the gamma order  $\alpha$  is plotted against the window width  $T'$  in operational time (left) and number of trials  $N$  (right). As a first result, it turned out that the error in estimating both

variables, CV<sup>2</sup> as well as FF, scales approximately linearly with the inverse gamma order  $1/\alpha$ . Thus, processes that are inherently more variable due to their stochastic nature imply a larger variance in estimating that variability. A second result evident from Fig. 6 is the generally lower error associated with the estimation of CV<sup>2</sup> as compared to the FF. This is easily explained by the fact that we pool ISIs from all trials, which results in samples that are much larger than that of  $N$  spike counts measured from  $N$  repeated trials (see also Section 4).

When increasing the length  $T'$  of the observation window, the total number of intervals in all trials increases. This larger sample size resulted in a reduced uncertainty in estimating CV<sup>2</sup>. The error in FF, however, turned out to be independent of  $T'$  (within the range tested) as the number of counting samples  $N$  did not increase with observation time. As expected, an increasing number of trials equally reduced the estimation error of both FF and CV<sup>2</sup>.

### 3.2. Measuring irregularity in presence of rate modulation

In practice, a clean measurement of spike train irregularity using the squared coefficient of variation CV<sup>2</sup> is often impaired by dynamic changes of the neuron's firing rate influencing the length of individual inter-spike intervals. This typically results in some extra dispersion of the ISI distribution and, consequently, in an over-estimation of the CV<sup>2</sup>. By contrast, the distribution of spike counts (and, hence, the Fano factor FF) remains unaffected by rate modulations that repeat identically in each single trial. The obvious reason is that only the number, but not the individual timings of spikes enter the spike count statistics.

To quantify irregularity despite a temporal modulation of the neuron's firing rate we measured the CV<sup>2</sup> in operational time. Doing so requires two additional steps of analysis. First, we must obtain an empirical estimate  $\hat{\lambda}(t)$  of the underlying firing rate profile. Second, we need to transform time  $t \mapsto t'$  according to the empirical rate function as sketched in Fig. 1. Only then can we measure the variability of the intervals in operational time. The reliable estimation of the deterministic rate function is critical. After superimposing all spike trains of a particular trial ensemble, we used the method of kernel convolution (Nawrot et al., 1999; Parzen, 1962) with a symmetric kernel of triangular shape. The most important parameter of this method is the width of the kernel, which defines the temporal resolution of the estimate. To determine the optimal kernel width we used the iterative method described in Nawrot et al. (1999), an alternative method was suggested by Paulin and Hoffman (2001).

We tested the proposed procedure and assessed the quality of the resulting estimate of CV<sup>2</sup> using numerical simulations of rate modulated gamma processes. As intensity function  $\lambda(t)$  we chose a Gaussian response profile, superimposed on a stationary background, as depicted by the gray curve in Fig. 7b. Technically, we first simulated a gamma process of order  $\alpha = 4$  in operational time, i.e. with constant unit rate under equilibrium conditions. Fig. 7a shows an ensemble of 20 repeated realizations in operational time and the respective empirical interval distribution with CV<sup>2</sup> = 0.21. We then transformed the spike

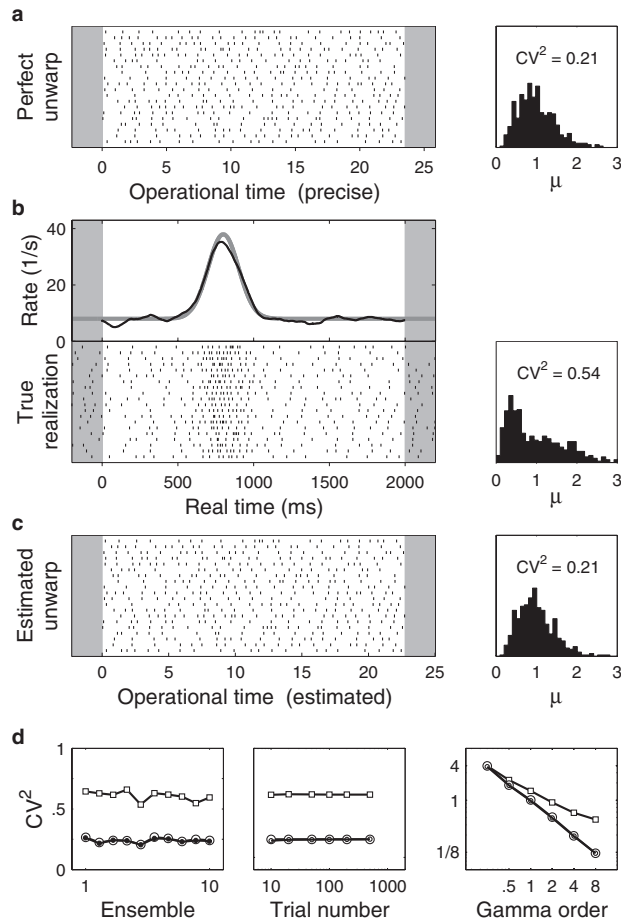


Fig. 7. Spike time irregularity quantified in operational time. (a) Raster diagram of 20 realizations of a gamma process ( $\alpha = 4$ ) simulated in operational time (left). The ISI distribution (right) is displayed in units of the mean interval  $\mu$ . (b) Spike density in real time follows the deterministic rate function (gray curve). The ISI distribution (right) is broadened by the non-stationarity of rate, leading to an over-estimation of the 'stationary' value of  $CV^2$ . (c) Spike trains after de-modulation according to the empirical rate estimate (black curve in (b)). The demodulated ISIs (right) match well the gamma distribution in (a). (d) In the left panel, the estimates of  $CV^2$  for true (open circles) and empirical (filled circles) operational time match well, as shown for 10 repeated simulations. By contrast, the modulated spike trains (open squares) consistently lead to a considerable over-estimation. This result is independent of the number of trials (middle panel). The positive estimation bias introduced by rate modulation is stronger for more regular processes (right).

trains to real time according to the intensity function  $\lambda(t)$ , as described by Eq. (4) and shown in Fig. 1.

The resulting set of 20 realizations is shown in the lower panel of Fig. 7b. Due to the temporal modulation of the firing rate we obtained an increased estimate of the irregularity  $CV^2 = 0.54$  in real time, which no longer reflected the imposed value of the underlying point process. To correct for this problem, we first estimated the rate function  $\hat{\lambda}(t)$  by averaging over trials as described above. Subsequent transformation from real time to estimated operational time resulted in the spike train ensemble shown in Fig. 7c. The measured value of  $CV^2 = 0.21$  was close to the correct value of the underlying stationary gamma process displayed in Fig. 7a. The number of trials entering the rate profile estimate did not significantly affect the outcome

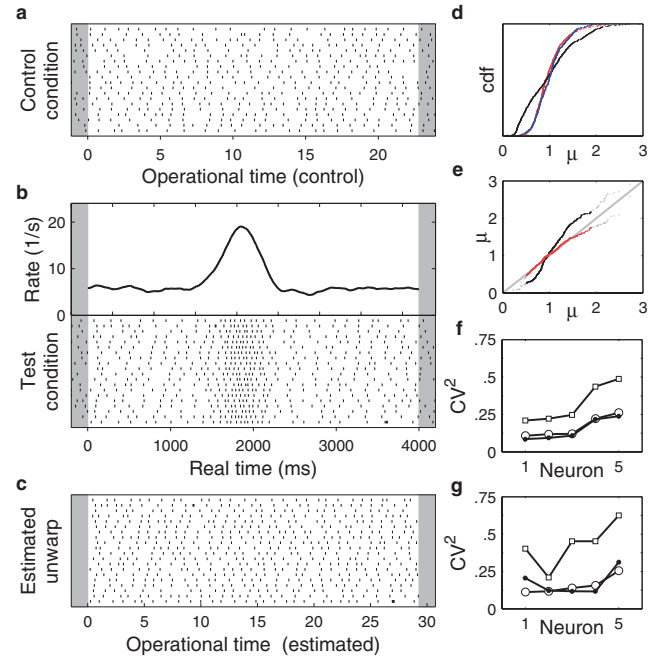


Fig. 8. De-modulation of spike trains. (a) Action potentials of one pyramidal neuron measured during 20 experimental control trials (stationary input condition) displayed in operational time. (b) The estimated rate function  $\hat{\lambda}(t)$  (black curve) from 20 spike trains recorded during test trials reflect the modulation of excitatory shotnoise input according to a Gaussian profile with 200 ms standard width. (c) Same spike train ensemble as in (b) after de-modulation of time using the transformation  $t \mapsto t'$  (Eq. (2), Fig. 1). (d) Estimated cumulative distribution functions (cdf) of ISIs relative to the mean interval  $\mu$  for control (blue), test (black) and de-modulated (red). (e)  $Q-Q$  plots of cumulative ISI distributions for test vs. control (black) and de-modulated vs. control (red). Colored values represent the 5%–95% inter-quantile range, gray values are outside this range. Repetition of the same experiment for 10 additional neurons for a modulation of standard width (f) 200 ms, and (g) 300 ms confirmed the good agreement of estimated  $CV^2$  in the control (open circles) and de-modulated test condition (filled circles). Open squares represent the rate modulated test condition.

of this procedure, as shown in the middle panel of Fig. 7d. We also verified the excellent performance of this procedure for processes of different gamma orders  $\alpha$  ranging from 0.5 to 8, as depicted in the right panel of Fig. 7d. We further tested the suggested procedure of measuring  $CV^2$  in rate modulated spike trains recorded from cortical pyramidal cells *in vitro*. As control condition we chose stationary shotnoise currents as input. The output rate of the neuron was constant, as shown in Fig. 8a. The operational time axis was scaled to unit rate, using the number of spikes during the observation interval (4 s) averaged across all trials. The resulting ISI distribution yielded  $CV^2 = 0.12$ . In the test condition, the neurons were stimulated with non-stationary shotnoise, where the excitatory component was enhanced by an extra Gaussian profile while the inhibitory input was unchanged with respect to the control condition (see Section 2). The spike trains extracted from 20 repeated measurements in one cell are shown in Fig. 8b. The ISI distribution of the non-stationary spike trains yielded  $CV^2 = 0.31$ , representing an increase of the irregularity by a factor close to 3 with respect to the control condition. De-modulation of the spike trains based on an estimate of the rate function  $\hat{\lambda}(t)$  resulted in a spike train ensemble of constant rate (Fig. 8c) and an ISI dis-

tribution with  $CV^2 = 0.11$ , in good agreement with the control condition.

In Fig. 8d we show the cumulative ISI distribution of the test (black), the control (blue), and the de-modulated (red) condition in operational time. The latter two match closely. In the quantile–quantile ( $Q-Q$ ) plot (Barbieri et al., 2001; Brown et al., 2001) in Fig. 8e we scattered the cumulative ISI distributions of the test condition against the control condition (red curve). The resulting curve coincides well with the diagonal, indicating very good agreement between the reconstructed and the true ISI distribution. Repetition of this experiment in 10 different neurons with either a Gaussian input profile of standard width 200 ms ( $N = 5$ , Fig. 8f) or 300 ms ( $N = 5$ , Fig. 8g) yielded equally good results.

A certain minimum number of independent trials is required to obtain a reliable estimate of the unconditional rate function. In addition, the process under observation must be in equilibrium, a requirement met in our simulations as well as in our *in vitro* experiments (see Section 4). In practice, due to time limitations in the experiments, the number of trials is typically of the order of only a few trials up to several hundreds, depending on the experiment design. In Fig. 7d we demonstrated that, for the tested gamma process and for the spike rates imposed, the value of  $CV^2$  can be safely estimated from a minimum of 10 trials. Generally, however, a low number of trials will yield a low total number of spikes. This has the same effect as low firing rates: The temporal resolution of the rate estimate is limited, and fast rate dynamics cannot be captured adequately (Nawrot et al., 1999). As a consequence, the de-modulation to operational time will not completely compensate modulations of the ISIs, and the irregularity of intervals is likely to be over-estimated. By contrast, over-compensation of rate fluctuations may occur if the kernel used for rate estimation is chosen too narrow, implying an inappropriately high temporal resolution.

### 3.3. Irregularity vs. count variability

Thus far we discussed the separate estimation of either irregularity or count variability. According to point process theory, however, inter-spike interval irregularity ( $CV^2$ ) and spike count variability (FF) are closely related. This suggests the co-analysis of both measures in neuronal spike data.

For stationary renewal processes, the prediction  $FF = CV^2$  holds for long observations, under only very mild assumptions on the process. We tested this prediction in our recordings from layer 5 pyramidal neurons *in vitro* while injecting either purely excitatory or balanced excitatory/inhibitory shotnoise currents. We therefore divided the total recorded spike train of several hundred seconds duration into trials of equal length. To avoid a significant estimation bias, we chose a fixed trial length of  $T' = 10$  in operational time, i.e. each trial comprised 10 spikes on average. We then computed the Fano factor of the spike counts, and the squared coefficient of variation of the ISIs from ensembles of  $N = 15$  trials. This is a trial number that we can realistically also expect to obtain in the case of more complicated experiments in behaving animals.

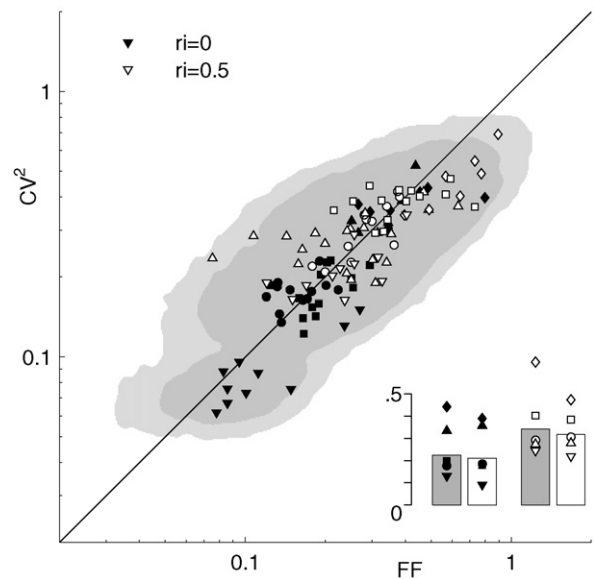


Fig. 9. Interval variability vs. count variability. Estimated FF and  $CV^2$  from ensembles of 15 trials and for a mean spike count of 10 (see text). Recordings are from the same five neurons (different symbols) as shown in Figs. 4 and 5, for two different current stimuli with either balanced input ( $r_i = 0.5$ , open symbols) or purely excitatory input (solid symbols). Dark and light gray shading represent 95% and 99% confidence regions from numerical simulations of gamma renewal processes; 108 of total 111 data points fall within the 95% region. Inset shows average values of FF (gray) and  $CV^2$  (white) for both input conditions. Symbols indicate averages for individual neurons.

The results for five neurons recorded under the two aforementioned conditions are shown in Fig. 9, where FF was scattered against  $CV^2$ . Each data point represents one ensemble of trials, open symbols stand for pure excitation ( $n = 48$ ), filled symbols stand for balanced excitation/inhibition ( $n = 63$ ). In the mean across all samples both measures of FF and  $CV^2$  are approximately equal with  $\langle FF \rangle = 0.29$  (geometric mean 0.25) and  $\langle CV^2 \rangle = 0.27$  (geometric mean 0.24). For purely excitatory input the neuronal responses were more regular and exhibited less trial-by-trial variability of their spike counts than for balanced input, as shown in the inset of Fig. 9. The individual estimates scatter around the identity line indicating  $FF = CV^2$ . This variability largely represents the uncertainty of the estimator due to a limited number of trials (cf. Fig. 6) and, as expected, for individual neurons the variance of estimation is typically larger for the FF. To verify this we again performed numeric simulations of gamma processes. For each data point we estimated the corresponding gamma order by  $\alpha = 1/CV^2$  (see Section 2) and repeatedly simulated ensembles of 15 trials with an expected mean count of 10 spikes. From the resulting simulations we constructed the 95% and 99% confidence regions, indicated in Fig. 9 by dark gray and light gray shading, respectively.

Our results show that the responses of cortical neurons recorded under stationary input conditions *in vitro* are in very good agreement with the predictions from renewal theory, with respect to second order interval and counting statistics. The variance in estimating FF and  $CV^2$  could be well predicted by numeric simulations of gamma-type renewal processes.

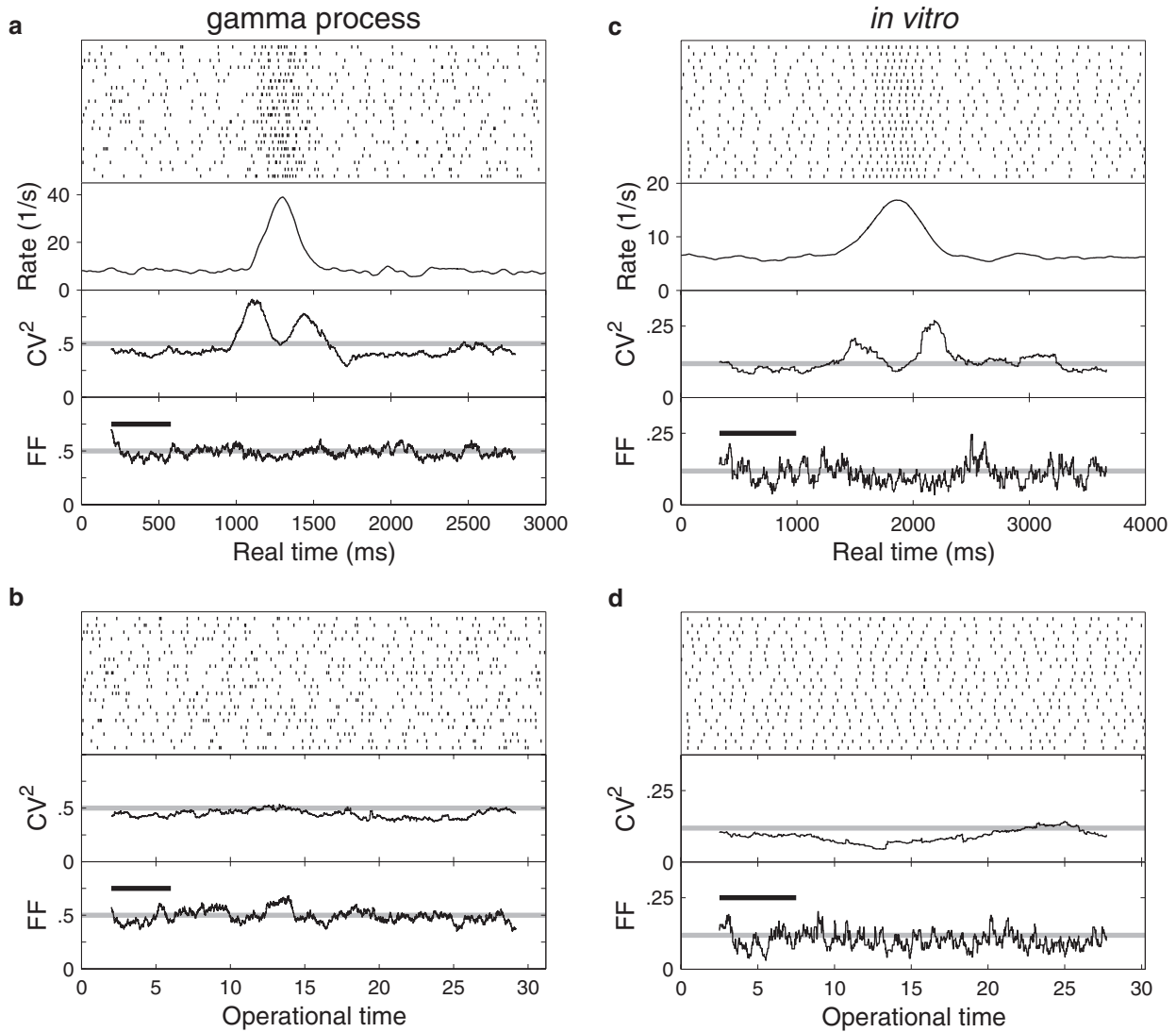


Fig. 10. Time resolved analysis of irregularity and variability. (a) Top panel shows 20 realizations of a rate modulated gamma process ( $\alpha = 2$ ) in real time. Empirical estimates of rate function,  $CV^2$  and FF are based on 100 trials, respectively. The horizontal bar indicates the analysis window of width  $T = 385$  ms. The gray horizontal line shows the asymptotic value. (b) De-modulated spike trains and time resolved measurement in operational time with a fixed window of length  $T' = 4$ . (c) Spike output of a cortical neuron during 20 repeated trials of modulated input current and time resolved measurement of  $CV^2$  and FF ( $T = 661$  ms). The gray line represents the empiric values as estimated during 20 control trials (see Section 2). (d) Demodulated spike trains as in b with  $T' = 5$ .

### 3.4. Time resolved joint analysis of irregularity and count variability

To study dynamic changes of neuronal variability we measured the  $CV^2$  and the FF in a sliding window of length  $T$ . The time resolved Fano factor has been employed in the analysis of experimental data in several earlier studies (Kara et al., 2000; Nawrot et al., 2003a; Oram et al., 2001). In practice, it is desirable to measure dynamic changes of variability with a time resolution  $T$  that also captures the relevant rate dynamics. In case of short analysis windows chosen for the sake of high temporal resolution this might result in a considerable estimation bias for both  $CV^2$  and FF, as discussed before. In general, this bias will change in time since for a non-stationary rate  $\lambda(t)$  a fixed window width  $T$  in real time translates into a variable interval  $T'$  in operational time. However, in operational time we can expect

this bias to stay constant which enables a faithful assessment of the temporal changes of spike train irregularity and spike count variability.

#### 3.4.1. Rate modulated gamma simulation

We first demonstrate the performance of this procedure in numerical simulations. Each spike train depicted in Fig. 10a presents one realization of a rate modulated gamma process with the same intensity function as in Fig. 7b. The time resolved measurement of  $CV^2(t)$  in Fig. 10a is badly corrupted. We observe a strong modulation, coinciding with the bell shaped rate response. As expected, the absolute value is highest where the change in rate  $d\lambda(t)/dt$  and, thus, the modulation of the ISIs is strongest. In addition, we observe a bias leading to a slight under-estimation of the theoretical expectation value  $CV^2_\infty = 1/\alpha = 0.5$  (gray line) during the early and late phase of the trial. This effect is

explained by the rather short analysis window of  $T = 385$  ms, equivalent to an average of  $T' = 4$  in operational time. After transformation to operational time (Eq. (2)) on the basis of the empirical rate function  $\hat{\lambda}(t)$  displayed in Fig. 10a, the resulting function  $CV^2(t)$  as measured in a window of width  $T' = 4$  is flat, as shown in Fig. 10b. Also, the bias is now reduced and constant throughout the trial.

The influence of rate modulation on the time resolved measurement of  $FF(t)$  in real time is explained by the estimation bias according to the calibration curve depicted in Fig. 5. During a phase of low rate the bias was relatively high, for high rate the bias was reduced. This bias-induced modulation is barely visible in the bottom curve of Fig. 10a as the analysis window was of sufficient length to avoid a significant bias. In operational time, the bias again remained constant over time by construction (Fig. 10b).

### 3.4.2. Modulated synaptic input currents *in vitro*

We repeated the time resolved measurement for a sample of our *in vitro* data, where the excitatory shotnoise input was modulated following a bell shaped profile (see Section 2). This resulted in a similar bell shaped modulation of the neuronal firing rate, as depicted in Fig. 10c. As for the model simulations, the dynamic changes of the  $CV^2$  suggest a strong modulation and an overall increase of spiking irregularity. However, in operational time, this effect is annihilated (Fig. 10d). Rather, the neuron now exhibited a slight reduction of  $CV^2$ . This shows that the irregularity is actually slightly reduced during the period of increased excitatory drive. This result is consistent with the observation that unbalancing of excitation and inhibition towards more excitation results in a more regular spike output of cortical layer 5 pyramidal neurons (cf. Fig. 9; Stevens and Zador, 1998).

### 3.4.3. Single unit recording in monkey motor cortex

Finally, we analyzed the task-related modulation of  $CV^2$  and  $FF$  in an example of an *in vivo* single neuron recording from the primary motor cortex of a monkey performing a center-out reaching task (see Section 2). In each experimental trial, the monkey was presented with a preparatory signal (PS) at time  $t = 0$  which indicated the required movement direction, which was chosen randomly as 1 out of 6 possible direction targets. The monkey was not allowed to move his hand from the central resting point, however, before the reaction signal (RS) appeared after a variable preparatory period of either 600 ms or 1200 ms which was chosen at random. The spike raster in Fig. 11a shows the recorded spike activity during 19 trials of one specific movement direction and for the short preparatory period of 600 ms. Trials were aligned to PS. Movement onset (MO) is indicated in each trial by a blue circle. Short before MO the neuron's firing rate shows a movement-related peak which is direction dependent (not shown).

The time-resolved measurements of  $FF$  and  $CV^2$  reveal task-related modulations of variability in Fig. 11c–f. The blue curves show the estimate on the original time axis of the experiment, the red curves show the estimate in operational time after back-transformation to the experimental time axis according to Eq. (4).

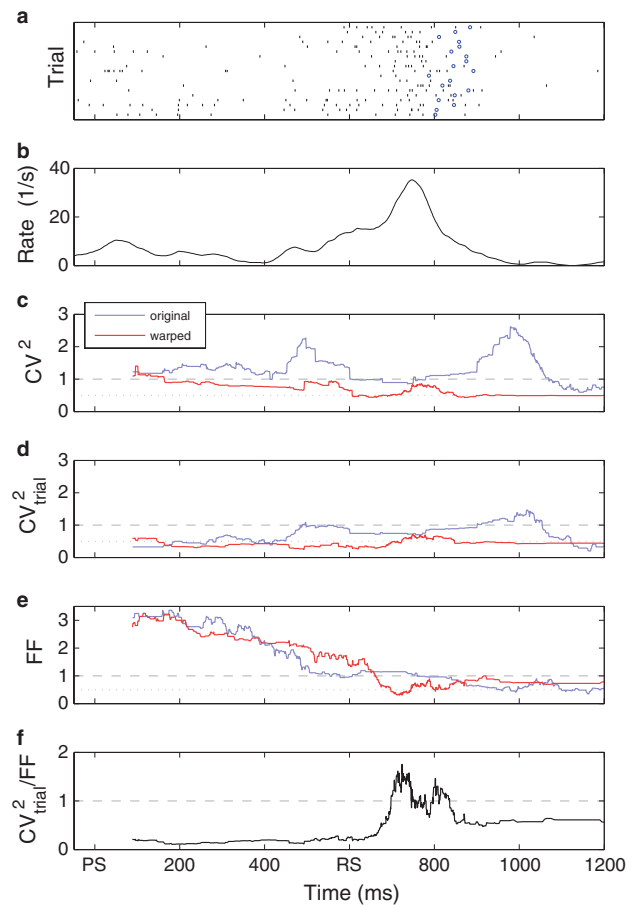


Fig. 11. Task-related changes of variability in monkey motor cortex. (a) Spiking activity of a motor cortical neuron during repeated trials which were aligned to the preparatory signal (PS) at time  $t = 0$ . Blue circles indicate the time of movement onset. (b) Estimated firing rate shows clear task-related modulation with a strong response shortly before movement onset. (c–f) Blue curves show variability measured in original time (window width  $T = 590$  ms), red curves show variability as measured in operational time ( $T' = 5$ ) after back-transformation to the experimental time axis. (c) The  $CV^2$  exhibits modulations in relation to rate changes when measured on the original time axis (blue). These modulations are largely diminished when measured in operational time (red) with mean  $CV^2 = 0.69$  smaller than unity. (d) Measuring the  $CV^2$  in each trial separately (see text) leads to a significantly reduced trial-averaged  $CV^2_{\text{trial}}$  which now appears to be almost constant throughout the task with an average of 0.50 in operational time (red). (e) Task-related Fano factor is highest at the beginning of the task but strongly decreases during the period of movement preparation. At the rate response peak shortly before onset of the center-out movement the Fano factor reaches a minimum at  $FF \approx 0.5$ – $0.6$ . (f) The ratio of  $CV^2_{\text{trial}}$  and  $FF$ , both measured in operational time, is close to unity during the task-related rate response.

Spike train irregularity in Fig. 11c measured in experimental time exhibits strong rate-related modulations, as expected. Measurement in operational time (red curve) yields a  $CV^2$  that is smaller than unity throughout the trial. In Fig. 11d we used a different estimator for the irregularity. Rather than pooling intervals from all trials, we now measured the  $CV^2_i$  in each trial  $i$  separately and then computed the trial-averaged  $CV^2_{\text{trial}}$ . This lead to further reduction to an almost constant value (average  $CV^2_{\text{trial}} = 0.50$ ).

Trial-by-trial count variability in Fig. 11e is large in the initial phase of the experiment with  $FF > 3$  but decreases throughout

the period of movement preparation. During the movement-related activity the Fano factor reaches a minimum at  $FF \approx 0.5$ – $0.6$ . This result is consistent with previous findings of task-modulated trial-by-trial variability in motor cortical neurons (Churchland et al., 2006; Nawrot et al., 2001, 2003a).

Thus, during the actual task-relevant and directionally tuned response both measures of trial-by-trial count variability and spike train irregularity are smaller than unity and become approximately equal with values around  $FF \approx CV^2 \approx 0.5$  (cf. Fig. 11f). The constant low value of  $CV^2_{\text{trial}} \approx 0.4$ – $0.6$  indicates that the nature of this neuron is less variable than a Poisson process.

## 4. Discussion

### 4.1. Operational time vs. real time

Observing a point process in finite windows may be associated with a considerable bias in the estimation of spike train irregularity,  $CV^2$ , and spike count variability,  $FF$ , with respect to the theoretical value assumed in the limit of infinite observation length. Our results from the analytical treatment of renewal processes were confirmed in numeric simulations of gamma-type renewal processes. The observed bias was found to depend on the length of the observation in operational time, i.e. on the expected spike count within that interval. From a theoretical point of view it is, thus, of advantage to estimate  $CV^2$  and  $FF$  in operational time rather than in real time.

Analysis of spike trains recorded from cortical pyramidal neurons under stationary input conditions *in vitro* confirmed the same bias dependencies of  $CV^2$  and  $FF$  on the mean spike count (cf. Figs. 4 and 5). In the case of non-constant firing rate profiles we suggested to de-modulate the spike trains by using a non-linear transformation of real time to operational time (Eq. (2)). This enables the time resolved analysis of spike train irregularity and trial-by-trial count variability. Back-transformation from operational to real time (Eq. (4), Fig. 11) allows for a comparison of the time resolved variability to other observables in real time.

The estimation bias of measuring variability in experimental spike trains has practical consequences. First of all, it is desirable to avoid a significant bias by choosing sufficiently long observation intervals. Our calibrations of the gamma-type renewal process and of experimental spike trains *in vitro* suggest to use windows that comprise not less than 5–10 spikes on average. A number of previous experimental as well as model studies have analyzed interval or count variability in considerably shorter windows (e.g. Amarasingham et al., 2006; Britten et al., 1993; Churchland et al., 2006; Dean, 1981; Geisler and Albrecht, 1997; Kara et al., 2000; Kargo and Nitz, 2004; Lee et al., 1998; Mazurek and Shadlen, 2002; Murthy and Fetz, 1996; Snowden et al., 1992; Vogels and Orban, 1991; Vogels et al., 1989). In a few examples the mean count was as small as  $T' \approx 0.1$ – $0.5$  and thus parts of the results are likely to be affected by a strong estimation bias.

Under certain circumstances we cannot avoid short observations, in particular for the time resolved analysis of variability

dynamics. We may then use the calibration curves (cf. Figs. 4 and 5) to obtain an estimate of and possibly correct for the introduced error. The more practical decision is to accept a certain bias which, for a fixed observation length in operational time, can be assumed to be constant and allow for a fair comparison of second order count and interval statistics across time and among different data samples (cf. Figs. 10 and 11). However, this condition often was not considered in earlier studies (see also discussion in Wiener, 2003 and Chelvanayagam and Vidyasagar, 2006). In several examples spike count variability in a single neuron was compared for different experimental conditions, implying that different firing rates and/or different observation windows were used (e.g. Kara et al., 2000; Kargo and Nitz, 2004; Mazurek and Shadlen, 2002; Murthy and Fetz, 1996). The same criticism applies to studies that compared variability of different neurons that exhibited different firing rates in a fixed time window (e.g. Kara et al., 2000; Lee et al., 1998; Oram et al., 2001). A series of studies that investigated cortical trial-by-trial variability first normalized the spike count to obtain an estimate of the spike rate, and only then computed the trial-by-trial standard deviation and the coefficient of variation of the rate variable (e.g. Lee et al., 1998; Maynard et al., 1999; Oram et al., 2001) or the trial-by-trial rate variance normalized by the mean rate (Churchland et al., 2006). When normalizing to rate, however, the information about spike count and interval duration is lost, and bias effects due to low spike counts are concealed. This marks the advantage of count-based statistics over rate-based statistics. Several studies investigated Fano factor vs. time curves  $FF(T)$  to characterize the spiking of cortical neurons (Baddeley et al., 1997; Buracas et al., 1998; Kara et al., 2000; Oram et al., 2001; Ratnam and Nelson, 2000; Teich et al., 1996). In all cases, however, this was studied in dependence on the width of the analysis window in real time rather than in operational time, which complicates the interpretation particularly for small values of  $T$ .

### 4.2. Renewal assumption

In this work, the analytic treatment and all numerical simulations were based on the model of a renewal process. A process which has dependent ISIs, however, violates this assumption and generally also exhibits a different behavior in its second order count and interval statistics. In particular, the equality  $FF = CV^2$  discussed in Eq. (5) holds only for independent intervals. A process with correlated ISIs (but which is still stationary and in equilibrium) satisfies the slightly more general equality

$$\lim_{T \rightarrow \infty} FF = CV_{\text{th}}^2 \left[ 1 + 2 \sum_{i=1}^{\infty} \xi_i \right], \quad (11)$$

where  $\xi_i$  denotes the  $i$ th order serial correlation coefficient, and  $CV_{\text{th}}^2$  is computed from the ‘theoretical’ ISI variance if all intervals were independent (Chacron et al., 2001; Cox and Lewis, 1966; Ratnam and Nelson, 2000).

We showed elsewhere (Nawrot et al., 2007) that the spontaneous activity of neocortical neurons recorded in the anesthetized rat typically exhibited a moderate negative correlation

coefficient for consecutive intervals ( $\xi_1 < 0$ ), but no significant correlation for higher-order pairs ( $\xi_i \approx 0$  for  $i \geq 2$ ). This result could be well explained by the same cellular mechanisms that are also responsible for spike frequency adaptation. The observed negative ISI correlation lead to an empirical FF that was reduced in comparison to a renewal control of randomly shuffled ISIs, and also smaller than the empirical  $CV^2$ , in accordance with Eq. (11). Layer 5 pyramidal neurons *in vitro* stimulated by noise current injection showed only a relatively weak negative first order serial correlation (Nawrot et al., 2007). Such ‘small deviations’ from the renewal model did not significantly affect the equality  $FF = CV^2$ , which still agreed well with the prediction from gamma renewal processes (cf. Fig. 9).

#### 4.3. Equilibrium condition

In this work, we treated renewal processes in equilibrium. This means that our observation started at a ‘random point’ with respect to the realization of the process, as if the process had been running for a long time already. In an ‘ordinary’ renewal process, by contrast, each observation (‘trial’) begins with a spike. In this case (and generally for processes that are not in equilibrium), the bias of FF and  $CV^2$  for short windows is altered due to artificial onset synchronization. Somewhat larger observation intervals are then required for a reliable empirical estimate (data not shown).

It depends on the experimental protocol whether the equilibrium or the ordinary renewal model more adequately describes the observed neuronal responses. The former might apply to experimental settings with a certain level of spontaneous spiking and smooth changes of activity associated with sensory input or motor output. However, in the case of low spontaneous activity and a sharp response onset that is tightly locked to the stimulus or behavioral event, the latter might be a more adequate descriptor. Similarly, the intracellular injection of a current step can lead to a sharp onset-locking of the leading spike which closely resembles an ordinary process.

In our *in vitro* experiments it was important to allow the recorded neuron to settle in a state of equilibrium after having started the somatic current injection. The onset of the shotnoise current, in fact, had severe effects on the neuron’s internal state. It induced a transition from rest to an active state. At rest the neuron received only negligible synaptic input due to sparse spontaneous activity typical for acute neocortical slices. The active state, by contrast, was associated with a net depolarization and strong fluctuations of the membrane potential, and with the generation of action potentials at a moderate rate. To exclude any transient or adaptation phenomena, our experimental protocol allowed for a long ( $> 50$  s) initial period of continuous injection of the synthetic fluctuating current before we started to analyze the data, and the stimulation was never halted throughout the experiment. This procedure is distinct from protocols that had been used in several previous *in vitro* studies of interval and count variability in cortical neurons (Harsch and Robinson, 2000; Nowak et al., 1997; Stevens and Zador, 1998). In these studies, current injection went through cycles of stimulation alternating with pauses of no stimulation, leading to fast input

transients at the beginning of each trial and a typical trial duration of only a few seconds.

#### 4.4. Refractory period

Our analytical results for non-stationary renewal processes were based on the assumption that the process dynamics is consistent with the notion of ‘operational time’, as expressed by Eq. (2). In real neurons, however, some aspects of the dynamics may be incompatible with the associated transformation. One candidate for this kind of problem is the absolute refractory time of neurons, which is fixed in real time since it is the result of sodium channel inactivation. The associated ‘dead time’ following each spike of the neuron does not scale with the firing rate, and hence it does not transform well to operational time (Berry and Meister, 1998; Kara et al., 2000; Reich et al., 1998; Teich et al., 1997). If we ignore this problem, we obviously violate the constraint of a fixed dead time and, consequently, introduce a (small) error in our estimate of the  $CV^2$  in operational time. This error will, however, increase with increasing rate. This was recently demonstrated for a related measure of interval variability by Chelvanayagam and Vidyasagar (2006). In cortical neurons where the dead time is small (a few milliseconds) this effect may be neglected as long as the ISIs are long (tens or hundreds of milliseconds).

#### 4.5. Non-stationarity across trials

An empirical estimate of the temporal firing rate profile is commonly obtained from experimental data by means of a trial averaging procedure, e.g. the PSTH. Doing so makes the implicit assumption that the rate function is the same in all trials, because only then the trial averaged estimate faithfully reflects the rate profile which underlies the generation of action potentials in individual trials (Aertsen et al., 1989; Knoblauch and Palm, 2005; Masuda and Aihara, 2003; Ventura et al., 2005). This criterion was clearly met in all our simulations where we imposed the same intensity function in all trials. Thus, the statistical variations in spike count and in ISI length were only due to the stochastic nature of the point process.

In our *in vitro* experiments the statistical fluctuations in the spike responses were due to a combination of stochastic external inputs and noise intrinsic to the neuron. The fluctuations of the input current were matched to mimic the activity of a large presynaptic population following some predefined rate profile, which was strictly the same in all trials. In the living brain, however, the level of input that a neuron receives may vary from trial to trial even if experimental conditions are unchanged. In the context of point process models, this can be interpreted as a trial-to-trial change of the underlying firing rate, either due to variations of the stimulus-related input or to changes of ongoing activity that are not locked to the time frame of the experiment (Arieli et al., 1996; Azouz and Gray, 1999; Kisley and Gerstein, 1999; Nawrot, 2003; Nawrot et al., 2001). This obfuscates a faithful estimation of the rate function by any procedure that relies on trial averaging. One obvious problematic consequence of this is an imperfect de-modulation

of the single-trial spike trains (Eq. (4)) and an over-dispersed ISI distribution.

In cases where non-stationary firing rate profiles across trials are suspected it may be useful to obtain an individual estimate of the  $CV^2$  in each trial and only then average across trials, rather than pooling the ISIs from all trials (cf. Fig. 11). This is equivalent to normalizing by the total spike count on a trial-to-trial basis. This procedure diminishes but cannot completely abolish the effect of trial-by-trial changes of firing rate. A similar strategy was recently followed by Davies et al. (2006). They introduced a new local metric for measuring irregularity, which was normalized separately in each trial. In a second step, averaging in time and across trials was performed. Trial-to-trial changes in firing rate has an even stronger increasing effect on the spike count variance, and thus on the Fano factor. For the co-analysis of both types of variability we must therefore expect that  $FF > CV^2$ . In fact, one can make use of this non-identity of  $FF$  and  $CV^2$  as a quantitative measure for across-trial non-stationarities. In a next step one can develop a model of such non-stationarities, develop appropriate correction procedures and use those to test the model (Nawrot, 2003; Nawrot et al., 2001). The sample time-resolved variability analysis of the single unit recording from the motor cortex of the behaving monkey presented in Fig. 11 is suggestive of across-trial non-stationarity in the early part of the trial. Further investigation of the nature and possible mechanisms of this phenomenon is currently under way (Nawrot et al., in preparation).

A special case of across trial non-stationarity is caused by the misalignment of individual trials. Repeated trials recorded in one experiment need to be aligned in time with respect to a meaningful reference, such as the occurrence of a stimulus or a behavioral event. Trials may be misaligned if the observed brain processes result in a neuronal response of variable latency with respect to that particular trigger event (Baker and Gerstein, 2001; Bollimunta et al., 2007; Brody, 1999; Nawrot et al., 2003a; Ventura, 2004). In this case, the trial averaged rate estimate will be smeared out in time and, again, rate estimate and demodulation is imperfect. This leads to an over-dispersed ISI distribution and, therefore, to an increased value of the empirical  $CV^2$ . The Fano factor will also be affected if the observation interval falls into a period of significant rate change, effectively leading to a trial-by-trial non-stationarity of the rate and, consequently, to an artificially increased spike count variance (Nawrot et al., 2003a).

#### 4.6. Variability in cortical neurons

We showed that, in line with previous studies (Harsch and Robinson, 2000; Nawrot et al., 2003b; Stevens and Zador, 1998), regular spiking cortical pyramidal neurons *in vitro* stimulated with stationary realistic fluctuating current input exhibited moderate Fano factors in the range 0.2–0.5. These numbers are compatible with the spike train irregularity observed in similar recordings (Arsiero et al., 2007; Badoual et al., 2005; Harsch and Robinson, 2000; Holt et al., 1996; Nawrot et al., 2003b; Nowak et al., 1997; Stevens and Zador, 1998). Balancing excitatory and inhibitory inputs increased both the spike count interval

variability by approximately 30%, but did not disrupt the equality of the two parameters (cf. Fig. 9). Similarly, our *in vivo* recordings of stationary spontaneous activity of single cortical neurons in the anesthetized rat had shown moderate count and interval variability in the very same range (Nawrot et al., 2007). We conclude that, for stationary input conditions, cortical neurons are clearly less variable than the Poisson process, and that single-neuron spiking is better approximated by gamma renewal processes with order parameters in the range of 2–5. This result contradicts the high trial-by-trial variability measured in awake animals where single neurons were found to be more variable than the Poisson process ( $FF > 1$ ) in the visual (for references see Shadlen and Newsome, 1998; Teich et al., 1996) and motor areas (Lee et al., 1998; Maynard et al., 1999), with few exceptions (Amarasingham et al., 2006; Gur et al., 1997; Kara et al., 2000).

In this paper we outlined a strategy of data analysis that helps to identify sources that contribute to the observed high trial-by-trial variability of cortical single neuron output *in vivo*. It involves (1) the joint analysis of spike train irregularity ( $CV^2$ ) and trial-by-trial count variability ( $FF$ ) in operational time and (2) the investigation of the task-related dynamics of both aspects on the same time scale.

#### Acknowledgments

We thank Jan Benda, George Gerstein, Benjamin Staude and Mathias Bethge for valuable discussions. We gratefully acknowledge financial support of this work by the German Federal Ministry for Education and Research (BMBF, grant 01GQ0420 to the BCCN Freiburg). Additional funding was received from the DAAD (VR) and the Heidelberg Academy of Sciences and Humanities (MN).

#### References

- Aertsen AMHJ, Gerstein GL, Habib MK, Palm G. Dynamics of neuronal firing correlation: modulation of effective connectivity. *J Neurophysiol* 1989;61:900–17.
- Amarasingham A, Chen TL, Geman S, Harrison MT, Sheinberg DL. Spike count reliability and the Poisson hypothesis. *J Neurosci* 2006;26:801–9.
- Arieli A, Sterkin A, Grinvald A, Aertsen A. Dynamics of ongoing activity: explanation of the large variability in evoked cortical responses. *Science* 1996;273:1868–71.
- Arsiero M, Lüscher HR, Lundstrom BN, Giugliano M. The impact of input fluctuations on the frequency–current relationships of layer 5 pyramidal neurons in the rat medial prefrontal cortex. *J Neurosci* 2007;27:3274–84.
- Azouz R, Gray CM. Cellular mechanisms contributing to response variability of cortical neurons *in vivo*. *J Neurosci* 1999;19:2209–23.
- Baddeley R, Abbot LF, Booth MCA, Sengpiel F, Freeman T, Wakeman EA. Response of neurons in primary and inferior temporal visual cortex to natural scenes. *Proc R Soc Lond B* 1997;264:1775–83.
- Badoual M, Rudolph M, Piwkowska Z, Destexhe A, Bal T. High discharge variability in neurons driven by current noise. *Neurocomputing* 2005;65–66:493–8.
- Baker SN, Gerstein GL. Determination of response latency and its application to normalization of cross-correlation measures. *Neural Comput* 2001;13:1351–77.
- Baker SN, Lemon R. Precise spatiotemporal repeating patterns in monkey primary and supplementary motor areas occur at chance level. *J Neurophysiol* 2000;84:1770–80.

- Barbieri R, Quirk MC, Frank LM, Wilson MA, Brown EN. Construction and analysis of non-Poisson stimulus–response models of neural spiking activity. *J Neurosci Meth* 2001;105:25–37.
- Berry MJ, Meister M. Refractoriness and neural precision. *J Neurosci* 1998;18:2200–11.
- Bollimunta A, Knuth KH, Ding M. Trial-by-trial estimation of amplitude latency variability in neuronal spike trains. *J Neurosci Meth* 2007;160:163–70.
- Boucsein C, Nawrot MP, Rotter S, Aertsen A, Heck D. Controlling synaptic input patterns in vitro by dynamic photo stimulation. *J Neurophysiol* 2005;94:2948–58.
- Britten KH, Shadlen MN, Newsome WT, Movshon JA. Responses of neurons in macaque MT to stochastic motion signals. *Vis Neurosci* 1993;10:1157–69.
- Brody CD. Correlations without synchrony. *Neural Comput* 1999;11:1537–51.
- Brown EN, Barbieri R, Ventura V, Kaas RE, Frank LM. The time-rescaling theorem and its application to neural spike train data analysis. *Neural Comput* 2001;14:325–46.
- Buracas GT, Zador AM, DeWeese MR, Albright TD. Efficient discrimination of temporal patterns by motion-sensitive neurons in primate visual cortex. *Neuron* 1998;20:959–69.
- Burkitt AN. A review on the integrate-and-fire neuron model. I. Homogenous synaptic input. *Biol Cybern* 2006;95:1–19.
- Chacron MJ, Longtin A, Maler L. Negative interspike interval correlations increase the neuronal capacity for encoding time-dependent stimuli. *J Neurosci* 2001;21:5328–43.
- Chelvanayagam DK, Vidyasagar TR. Irregularity in neocortical spike trains: influence of measurement factors and another method of estimation. *J Neurosci Meth* 2006;157:264–73.
- Churchland MM, Yu BM, Ryu SI, Santhanam G, Shenoy KV. Neural variability in premotor cortex provides a signature of motor preparation. *J Neurosci* 2006;26:3697–712.
- Cox DR. Renewal theory. Science paperbacks. London: Chapman and Hall; 1962.
- Cox DR, Isham V. Point processes. Monographs on applied probability and statistics. Chapman and Hall; 1980.
- Cox DR, Lewis PAW. The statistical analysis of series of events Methuen's monographs on applied probability and statistics. London: Methuen; 1966.
- Davies RM, Gerstein GL, Baker SN. Measurement of time-dependent changes in the irregularity of neural spiking. *J Neurophysiol* 2006;96:906–18.
- Dean AF. The variability of discharge of simple cells in the cat striate cortex. *Exp Brain Res* 1981;44:437–40.
- Dotd HU, Zieglgänsberger W. Visualizing unstained neurons in living brain slices by infrared dic-videomikroskopie. *Brain Res* 1990;537:333–6.
- Fano U. Ionization yield of radiations. II. The fluctuations of the number of ions. *Phys Rev* 1947;72:26–9.
- Geisler WS, Albrecht DG. Visual cortex neurons in monkeys and cats: detection, discrimination, and identification. *Vis Neurosci* 1997;14:897–919.
- Gestri G, Petracchi D. The transformation induced by light stimulus on the retinal discharge: study of the interval distribution at high frequencies of sinusoidal stimulation. *Kybernetik* 1970;6:171–6.
- Grammont F, Riehle A. Spike synchronization and firing rate in a population of motor cortical neurons in relation to movement direction and reaction time. *Biol Cybern* 2003;88:360–73.
- Gur M, Beylin A, Snodderly M. Response variability of neurons in primary visual cortex (V1) of alert monkeys. *J Neurosci* 1997;17:2914–20.
- Harsch A, Robinson H. Postsynaptic variability of firing in rat cortical neurons: the roles of input synchronization and synaptic NMDA receptor conductance. *J Neurosci* 2000;20:6181–92.
- Holt GR, Softky WR, Koch C, Douglas RJ. Comparison of discharge variability in vitro and in vivo in cat visual cortex neurons. *J Neurophysiol* 1996;75:1806–14.
- Johnson DH. Point process models of single-neuron discharges. *J Comput Neurosci* 1996;3:275–99.
- Kara P, Reinagel P, Reid C. Low response variability in simultaneously recorded retinal, thalamic, and cortical neurons. *Neuron* 2000;27:635–46.
- Kargo WJ, Nitz DA. Improvements in the signal-to-noise ratio of motor cortex cells distinguish early versus late phases of motor skill learning. *J Neurosci* 2004;24:5560–9.
- Kass RE, Ventura V. A spike-train probability model. *Neural Comput* 2001;13:1713–20.
- Kisley M, Gerstein G. Trial-to-trial variability and state-dependent modulation of auditory-evoked responses in cortex. *J Neurosci* 1999;23:10451–60.
- Knoblauch A, Palm G. What is signal and what is noise in the brain? *BioSystems* 2005;79:83–90.
- Lee D, Port NL, Kruse W, Georgopoulos AP. Variability and correlated noise in the discharge of neurons in motor and parietal areas of the primate cortex. *J Neurosci* 1998;18:1161–70.
- Lindner B. Interspike interval statistics of neurons driven by colored noise. *Phys Rev E* 2004;69:0229011–4.
- Masuda N, Aihara K. Ergodicity of spike trains: when does trial averaging make sense? *Neural Comput* 2003;15:1341–72.
- Maynard EM, Hatsopoulos NG, Ojakangas CL, Acuna BD, Sanes JN, Normann RA. Neuronal interactions improve cortical population coding of movement direction. *J Neurosci* 1999;19:8083–93.
- Mazurek ME, Shadlen MN. Limits to the temporal fidelity of cortical spike rate signals. *Nat Neurosci* 2002;5:463–71.
- Meier R, Gruen S, Boucsein C, Aertsen A, Boven KH, Egert U. Characterizing neural network dynamics: analyzing neural activity data using the FIND-toolbox. No. 319.11. 2007. In: Neuroscience Meeting Planner. San Diego, CA: Society for Neuroscience; 2007. Online.
- Murthy VN, Fetz E. Synchronization of neurons during local field potential oscillations in sensorimotor cortex of awake monkeys. *J Neurophysiol* 1996;76:3968–82.
- Nawrot MP. Ongoing activity in cortical networks: noise, variability and context. PhD thesis. Faculty of Biology, Albert-Ludwigs-University Freiburg, Germany; 2003.
- Nawrot MP, Aertsen A, Rotter S. Single-trial estimation of neuronal firing rates: from single-neuron spike trains to population activity. *J Neurosci Meth* 1999;94:81–92.
- Nawrot MP, Aertsen A, Rotter S. Elimination of response latency variability in neuronal spike trains. *Biol Cybern* 2003a;88:321–34.
- Nawrot MP, Boucsein C, Rodriguez-Molina V, Aertsen A, Grün S, Rotter S. Serial interval statistics of spontaneous activity in cortical neurons in vivo and in vitro. *Neurocomputing* 2007;70:1717–22.
- Nawrot MP, Pistoht T, Schrader S, Hehl U, Rodriguez V, Aertsen A. Embedding living neurons into simulated neural networks. In: Proceedings of the 1st international IEEE EMBS conference on neural engineering; 2003b. p. 229–32.
- Nawrot MP, Rodriguez V, Heck D, Riehle A, Aertsen A, Rotter S. Trial-by-trial variability of spike trains in vivo and in vitro. *Soc Neurosci Abstr* 2001;27:64.9.
- Nowak LG, Sanchez-Vives MV, McCormick DA. Influence of low and high frequency inputs on spike timing in visual cortical neurons. *Cereb Cortex* 1997;7:487–501.
- Oata Y. Statistical models for earthquake occurrences and residual analysis for point processes. *J Am Statist Assoc* 1988;83:9–27.
- Oram MW, Hatsopoulos NG, Richmond BJ, Donoghue JP. Excess synchrony in motor cortical neurons provides redundant direction information with that from coarse temporal measures. *J Neurophysiol* 2001;86:1700–16.
- Oram MW, Wiener MC, Lestienne R, Richmond BJ. Stochastic nature of precisely timed spike patterns in visual system neuronal responses. *J Neurophysiol* 1999;81:3021–33.
- Parzen E. On estimation of a probability density function and mode. *Ann Math Stat* 1962;33:1065–76.
- Paulin MG, Hoffman LF. Optimal firing rate estimation. *Neural Networks* 2001;14:877–81.
- Pauluis Q, Baker SN. An accurate measure of the instantaneous discharge probability, with application to unitary joint-event analysis. *Neural Comput* 2000;12:647–69.
- Perkel DH, Gerstein GL, Moore GP. Neuronal spike trains and stochastic point processes. I. The single spike train. *Biophys J* 1967a;7:391–418.
- Perkel DH, Gerstein GL, Moore GP. Neuronal spike trains and stochastic point processes. II. Simultaneous spike trains. *Biophys J* 1967b;7:419–40.
- Prut I, Perlmutter SI. Firing properties of spinal interneurons during voluntary movement. I. State-dependent regularity of firing. *J Neurosci* 2003;29:9600–10.

- Ratnam R, Nelson ME. Nonrenewal statistics of electrosensory afferent spike trains: implications for the detection of weak sensory signals. *J Neurosci* 2000;20:6672–83.
- Reich DS, Victor JD, Knight BW. The power ratio and the interval map: spiking models and extracellular recordings. *J Neurosci* 1998;18:10090–104.
- Ripley BD. *Stochastic simulation Wiley series in probability and mathematical statistics*. New York: John Wiley & Sons; 1987.
- Rotter S, Riehle A, Rodriguez-Molina V, Aertsen A, Nawrot MP. Different time scales of spike train variability in motor cortex. Program No. 276.7. 2005. In: *Abstract Viewer/Itinerary Planner*. Washington, DC: Society for Neuroscience; 2005, Online.
- Shadlen MN, Newsome WT. The variable discharge of cortical neurons: implications for connectivity, computation, and information coding. *J Neurosci* 1998;18:3870–96.
- Snowden R, Treue S, Anderson R. The response of neurons in areas V1 and MT of the alert rhesus monkey to moving random dot patterns. *Exp Brain Res* 1992;88:389–400.
- Softky WR, Koch C. The highly irregular firing of cortical cells is inconsistent with temporal integration of random EPSPs. *J Neurosci* 1993;13:334–50.
- Stein RB. A theoretical analysis of neuronal variability. *Biophys J* 1965;5:173–94.
- Stein RB, Gossen ER, Jones KE. Neuronal variability: noise or part of the signal? *Nat Rev Neurosci* 2005;6:389–97.
- Stevens CF, Zador AM. Input synchrony and the irregular firing of cortical neurons. *Nat Neurosci* 1998;1:210–7.
- Teich MC, Heneghan C, Lowen SB, Ozaki T, Kaplan E. Fractal character of the neural spike train in the visual system of the cat. *J Opt Soc Am A* 1997;14:529–46.
- Teich MC, Turcott RG, Siegel RM. Temporal correlation in cat striate-cortex neural spike trains. *IEEE Eng Med Biol Mag* 1996;15:79–87.
- Truccolo W, Eden UT, Fellows MR, Donoghue JP, Brown EN. A point process framework for relating neural spiking activity to spiking history, neural ensemble, and extrinsic covariate effects. *J Neurophysiol* 2005;93:1074–89.
- Tuckwell HC. *Introduction to theoretical neurobiology*, vol. 2. Cambridge: Cambridge University Press; 1988.
- Ventura V. Testing for and estimating latency effects for poisson and non-poisson spike trains. *Neural Comput* 2004;16:2323–49.
- Ventura V, Cai C, Kass RE. Trial-to-trial variability and its effect on time-varying dependency between two neurons. *J Neurophysiol* 2005;94:2928–39.
- Vogels R, Orban G. Quantitative study of striate single unit responses in monkeys performing an orientation discrimination task. *Exp Brain Res* 1991;84:1–11.
- Vogels R, Spileers W, Orban G. The response variability of striate cortical neurons in the behaving monkey. *Exp Brain Res* 1989;77:432–6.
- Wiener MC. An adjustment of the time-rescaling method for application to short-trial spike train data. *Neural Comput* 2003;15:2565–76.